Energy Reports 7 (2021) 896–903

Contents lists available at ScienceDirect

Energy Reports

journal homepage: www.elsevier.com/locate/egyr

ZnO/PDMS nanocomposite generator: Interphase influence in the nanocomposite electro-mechanical properties and output voltage

Carlos Andres Perez-Lopez [a], Jaime Andres Perez-Taborda [a], Cilene Labre [b], Juan Manuel Marmolejo-Tejada [d], Andres Jaramillo-Botero [c,d], Alba Avila [a,*]

[a] Centro de Microelectrónica (CMUA), Departamento de Ingeniería Eléctrica y Electrónica, Universidad de los Andes, Bogotá, 111711, Colombia
[b] Centro Brasileiro de Pesquisas Fisicas, Rio de, Janeiro, 22290-180, Brazil
[c] Chemistry and Chemical Engineering division, California Institute of Technology, Pasadena, CA 91125, USA
[d] Departamento de Electrónica y Ciencias de la Computación, Pontificia Universidad Javeriana Cali, Cali, 760031, Colombia

ARTICLE INFO

Article history:
Received 6 November 2020
Received in revised form 22 January 2021
Accepted 25 January 2021
Available online xxxx

Keywords:
Interphase overlapping
Mechanoelectric energy conversion
Polymer composite

ABSTRACT

Nanocomposite generators convert mechanical energy into electrical energy and are attractive low-power solutions for self-powered sensors and wearables. Homogeneous dispersion, high concentration, and orientation of the embedded filler strategies have been assumed to maximize the voltage output in nanocomposite generators. This work contrast these assumptions by studying the dominance of the interphase in low filler concentrations (<10%) and random dispersions in a ZnO/PDMS nanocomposite generator with high peak-to-peak voltage generation capabilities (≈150 V). The interphase in the nanocomposite was studied by the analysis of the random dispersion of the nanocomposite through the estimation of the effective volume fraction (ϕ_{agg}) which allowed us to identify three levels of interaction: individual interphases, interacting interphases, and overlapping between NPs and interphases. The interacting interphase is responsible here for the high generated voltage. In addition, the impact of the interphase was studied by applying lumped element (LE) and interphasial power-law (IPL) models that capture the measured voltages and the electromechanical film properties. The obtained results justify that engineering of interphases could be a design strategy for high voltage generation.

1. Introduction

Zinc Oxide (ZnO) based nanocomposite generators transform mechanical energy into electrical energy and are attractive as low-power solutions for self-powered wearables and sensors (Chen and Wang, 2017; Song et al., 2019; Pradel et al., 2014; Xu et al., 2010). ZnO nanocomposite generators with improved piezoelectric response have been explored through multiple strategies: type of the embedded filler, homogeneous dispersion, high concentration, and high order orientation (Parangusan et al., 2017, 2018; Hasan et al., 2015; Kumar and Kim, 2012). However, other strategies that aim to improve the nanocomposite's properties and output voltage by the effect of the interphases and their interaction in random dispersion with aggregates and agglomerates are yet to be comprehensively studied. Previous studies have demonstrated that the interphase region where the filler affects the surrounding polymer plays a crucial role in properties of the nanocomposite (dielectric constant (Latif et al., 2013), electric displacement (Zhang et al., 2018), Young's modulus (Raja et al., 2015), tensile strength (Abbas et al., 2019)). However, there are no studies on the interphase and interphase interaction effect on the output voltage on piezoelectric nanocomposite generators.

Although the interphase size and property measurement are rather challenging to detect at low filler concentrations and with direct non-invasive techniques that could impact the nanocomposite generator performance (Netravali and Mittal, 2017), indirect techniques can be used to deduce the interphase volume and properties by analyzing differences in the nanocomposite electromechanical properties at different conditions of filler concentration and dispersion (Netravali and Mittal, 2017). In these indirect techniques, the interphase size can be estimated by the effective volume fraction (ϕ_{agg}) that accounts for the total fraction of the interphase's volume in the nanocomposite (Jang et al., 2012; Zare, 2016). Comprehensive understanding of the interphase-based mathematical frameworks allowed the identification of three levels of interactions in polymer nanocomposites (Liu et al., 2016):

- Individual interphase regions, when the distance between NPs is high due to the effect of a homogenous dispersion or low concentrations and causes the interphases to be isolated from the others' effect resulting in low ϕ_{agg}.

* Corresponding author.
E-mail address: a-avila@uniandes.edu.co (A. Avila).

https://doi.org/10.1016/j.egyr.2021.01.086

- Interacting interphase regions, where the distance between NPs is reduced by the effect of increased concentration and random distribution causing the formation of aggregates and zones of interphase intersection, resulting in an increased ϕ_{agg} and higher contribution to the nanocomposite.
- Overlapping regions, where the distance NPs is reduced up to contact producing agglomerates and causing the NP volume to occupy the interphase decreasing ϕ_{agg} and the interphase effect to the nanocomposite.

At concentrations up to 7.4 wt%, the output is ruled by the interphase interactions, while at 9.1 wt% is affected by the overlapping between NPs and interphases. PDMS was selected due to optical transparency that allows filler aggregate observation, controlled cross-linking process which allows for repeatable processing, and because it has been proven to interact with ZnO ensuring the formation of an interphase (Bistričić et al., 2013). To achieve this, we have manufactured and analyzed five sets of ZnO nanocomposite films with filler concentration ranging from 2 wt% to 9.1 wt%, in addition to a pure PDMS sample. The ZnO NPs diameter distribution was determined by dynamic light scattering (DLS), the nanocomposites were characterized using impedance analysis, dynamic mechanical analysis (DMA), and transmission electron microscopy (TEM) to determine their electromechanical properties and filler dispersion respectively. Aggregate size analysis on microscopy analysis was used to estimate the ϕ_{Agg} parameter that represents the volume fraction of the nanocomposite occupied by the interphase. The impact of the interphase in the nanocomposite's electromechanical properties (ε_r and Y) was studied by applying an interphasial power-law (IPL) model that demonstrated the contribution of the interphases interactions and overlapping with NPs as a critical element to capture the measurements. An *in-house* experimental setup was used to measure the nanocomposite generator's capability to generate an electrical potential from mechanical excitations. A lumped element (LE) model defined in terms of the interphase dependent ε_r and Y was applied to identify their variation's effect on the voltage generation mechanism of the produced nanocomposite generator. These results demonstrate that for ZnO/PDMS nanocomposite generators, the interacting interphase strategy is a critical element in the design of interphasial characteristics for high voltage generation at low concentration and random dispersion conditions.

2. Materials and methods

Five sets of ZnO nanocomposite films with filler concentration ranging from 2 wt% to 9.1 wt% in addition to a pure PDMS film, were prepared following the procedure described in Fig. 1. Initially, the ZnO NPs powder (677450-5G, Sigma Aldrich) with 60 nm diameter (see supplementary materials, Figure S1) was mixed with the PDMS (Sylgard 184, Dow Corning) curing agent followed by a sonic bath for 30 min at 40 kHz. The mixture was then combined with the PDMS base agent at 10:1 ratio and degassed in vacuum (20 kPa) for 30 min to remove trapped air bubbles during PDMS mixing. Subsequently, the mixture was poured onto a copper tape adhered to a glass slide substrate (1181, 3M; 0313–2201, Citoglass) and then spin-coated at 1500 rpm for 1 min. Finally, the films were cured at 50 °C for 24 h and at 120 °C for 10 min to evaporate the solvent. A profilometer (Dektak 3, Veeco) was used to measure the film thickness of $25.5 \pm 3.4\,\mu$m.

2.1. Characterization of piezoelectric nanocomposite

The voltage and current response to the films' mechanical excitation was measured using a mixed-signal oscilloscope (MSO2024b, Tektronix). The excitation was applied by the *in-house* developed characterization setup for this measurement shown in Fig. 2(a) that is composed of a mechanical excitation unit, a sample holder, and a control unit, allowing the mechanoelectrical energy conversion characterization of nanocomposite generators.

A force excitation up to a 20.2 ± 0.2 N at 4 Hz was applied in tapping mode, out of plane direction by direct contact with a top plate which is displaced by a clamped steel bar that was coupled with the DC motor's shaft (37Dx57Lmm, Pololu). The sample holder's bottom side was screwed into the device's base plate, and the holder topside was attached to the spring-supported top electrode plate. In the top plate, aluminum tape was used as an electrode, providing improved charge transfer between the electrode and PDMS due to their different abilities to gain or lose charge when surfaces are in contact (Ding et al., 2018; Diaz and Felix-Navarro, 2004). The plate covers the entire area of the film (12.5 cm^2). The design allows the adjustment of the distance between the electrode and the film up to a height of 15 mm using set screw shaft collars. The effective surface resistance from which the induced force of 20.2 N is estimated by a force sensor (Flexiforce A201, Tekscan) placed underneath the ZnO nanocomposite. This force results from the contact of the steel bar attached to the motor's shaft from the top plate. For the reference background measurements, the film was removed, and then the applied force showed a variation of approximately 0.5 N. The forces were correlated to the generated voltage at each filler concentration once the films received mechanical excitation.

The control unit depicted in Fig. 2(a) includes a microcontroller (nano, Arduino), a Bluetooth communication module, and an H-bridge amplifier (IBT2). We developed an android app to send instructions to the microcontroller via Bluetooth (Avila et al., 2020); then, the microcontroller program sets the frequency of excitation of the nanocomposite generator. A video of the working *in-house* setup can be found in the supplementary information. Besides, a testing board (see Figs. 2(b) and 2(c)) with a full-wave rectifier and a three LEDs array (19-213USRC/S259 / TR8, Everlight Electronics) permits to inspect the nanocomposite film's response. The array was powered by the nanocomposite generator, demonstrating its real-time energy conversion capabilities.

2.2. Nanocomposite characterization

An Impedance analyzer (4294A, Agilent) with the Dielectric Test Fixture attachment (16451B, Agilent) was employed to estimate the ε_r value from the measured capacitance as a function of NPs concentration for frequencies ranging from 40 Hz to 1 kHz. The parameters of parallel capacitance (C_p) and parallel resistance (R_p) were measured at a bandwidth setting of 5, averaging a factor of 30, ambient temperature of 22 °C and 32% relative humidity. ε_r is estimated from C_p as stated in Eq. (1).

$$\varepsilon_r = \frac{tC_p}{\pi r^2 \varepsilon_0} \tag{1}$$

Where t is the film thickness ($25.5 \pm 3.4\,\mu$m), C_p is the measured parallel capacitance, r is the guarded electrode active radius (2.5 mm) and ε_0 corresponds to the vacuum permittivity (Technologies, 2014).

Regarding the characterization of the ZnO/PDMS nanocomposite, compositional and structural analysis was carried out by Raman spectroscopy (MicroRaman Jobin Yvon, Horiba) with a 532 nm Nd:YAG laser (8.5 mW), X-ray Photoelectron Spectroscopy (XPS) (hemispherical energy analyzer PHOIBOS 100/150, SPECS), and Transmission Electron Microscopy (TEM) (Titan G2 80–300, Thermo Fisher Scientific).

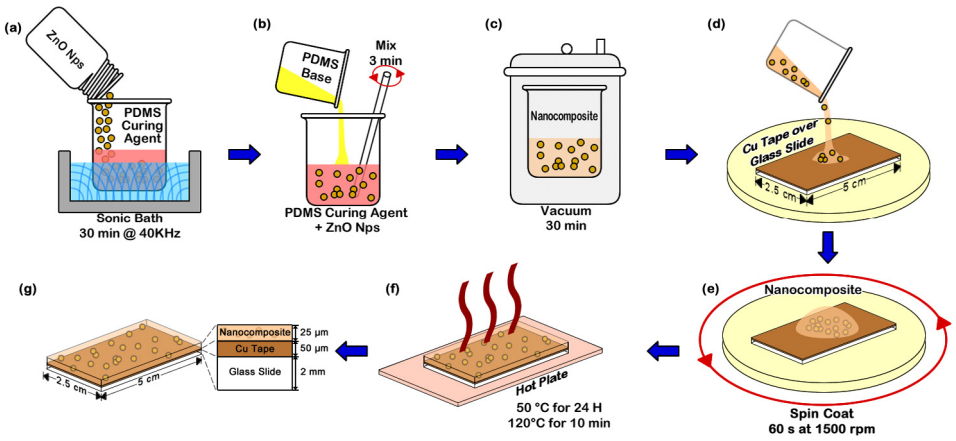

Fig. 1. Schematic diagram for the preparation of ZnO nanocomposite films: (a) mixing and sonication of ZnO NPs and PDMS curing Agent, (b) addition of PDMS base, (c) degassing, (d) pouring onto copper tape adhered on a glass slide, (e) spin coating, (f) solvent evaporation, (g) sample multilayering.

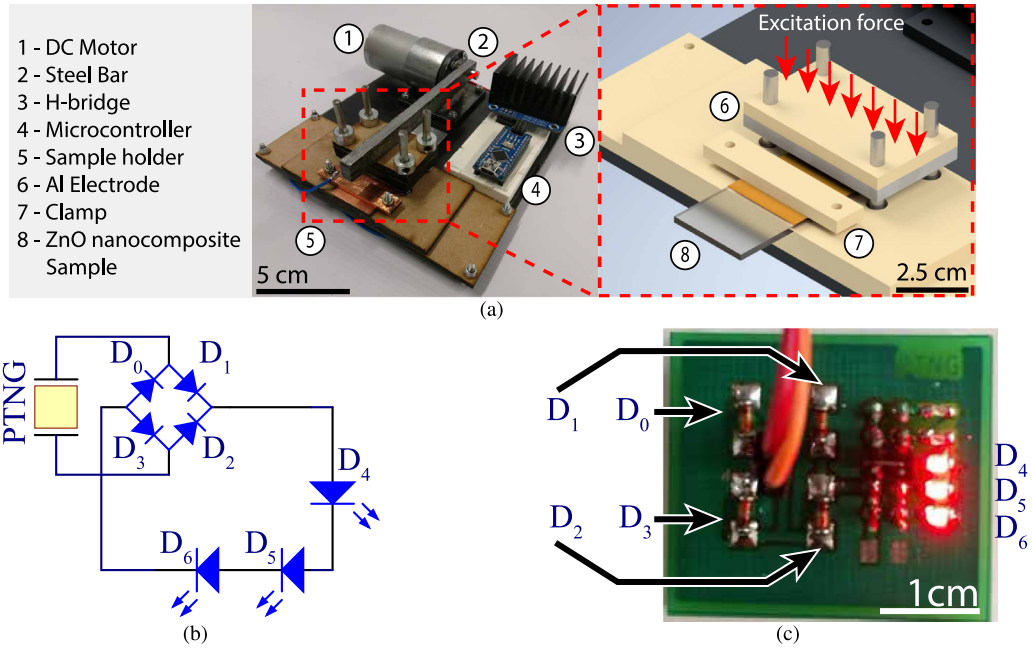

Fig. 2. Experimental setup for energy conversion test: (a) in-house setup: exciting and voltage acquisition units, the inset shows the sample holder: aluminum tape top electrode and nanocomposite generator on top of a glass slide (b) Testing board circuit schematic integrating a full bridge rectifier (D_0, D_1, D_2, D_3) and a three LEDs array (D_4, D_5, D_6), LEDs will turn on when the generated Voltage reaches the forward voltage of the series LED, (c) Testing board powered by a nanocomposite generator at 7.4 wt% ZnO NPs concentration, activated by an excitation force of 20.2 N at 4 Hz.

A dynamic mechanical analyzer (DMA) (Q800, TA Instruments) in tension mode with the linear film tension clamp was attached to a rectangular sample of the film (7 mm length by 8 mm width) at a force ramp of 0.5 N min^{-1} at 30 °C. Young's modulus Y was estimated by calculating the slope on the elastic region of the obtained stress vs strain curve.

ZnO NPs size distribution was determined from two techniques, namely dynamic light scattering (DLS) (Zetasizer Nano ZS, Malvern Panalytical) and Transmission Electron Microscopy (TEM) (Titan G2 80–300, Thermo Fisher Scientific). For the former, the ZnO NPs were suspended in tetramethylammonium hydroxide (TMAH) at 5 wt/vol%. For the later, a 120 nm slice of the ZnO nanocomposite sample was extracted using a Focused Ion Beam technique (FIB) lift-out technique (LYRA3, Tescan) (Giannuzzi et al., 1998). Distribution of ZnO aggregates was estimated by optical microscopy analysis using the particle analysis plugin on the Fiji software (Schindelin et al., 2012). Analyzed samples were obtained by delamination of the nanocomposite from the copper substrate.

3. Results and discussion

Figs. 3(a) and 3(b) show the voltage and current generated by the produced nanocomposite generators when connected to different resistance loads. The load corresponds to a resistance substitution box (236A, Phipps & Bird) with values ranging from 0.2 to 10 MΩ, connected to the nanocomposites electrodes. Measured voltages increase while currents decrease with the load resistance value. The nanocomposite with 7.4 wt% concentration exhibits the highest voltages and currents on all load resistances; this indicates that the filler concentration in a nanocomposite is related to the output voltage and that the nanocomposite properties at 7.4 wt% concentration allowed improved electromechanical energy conversion.

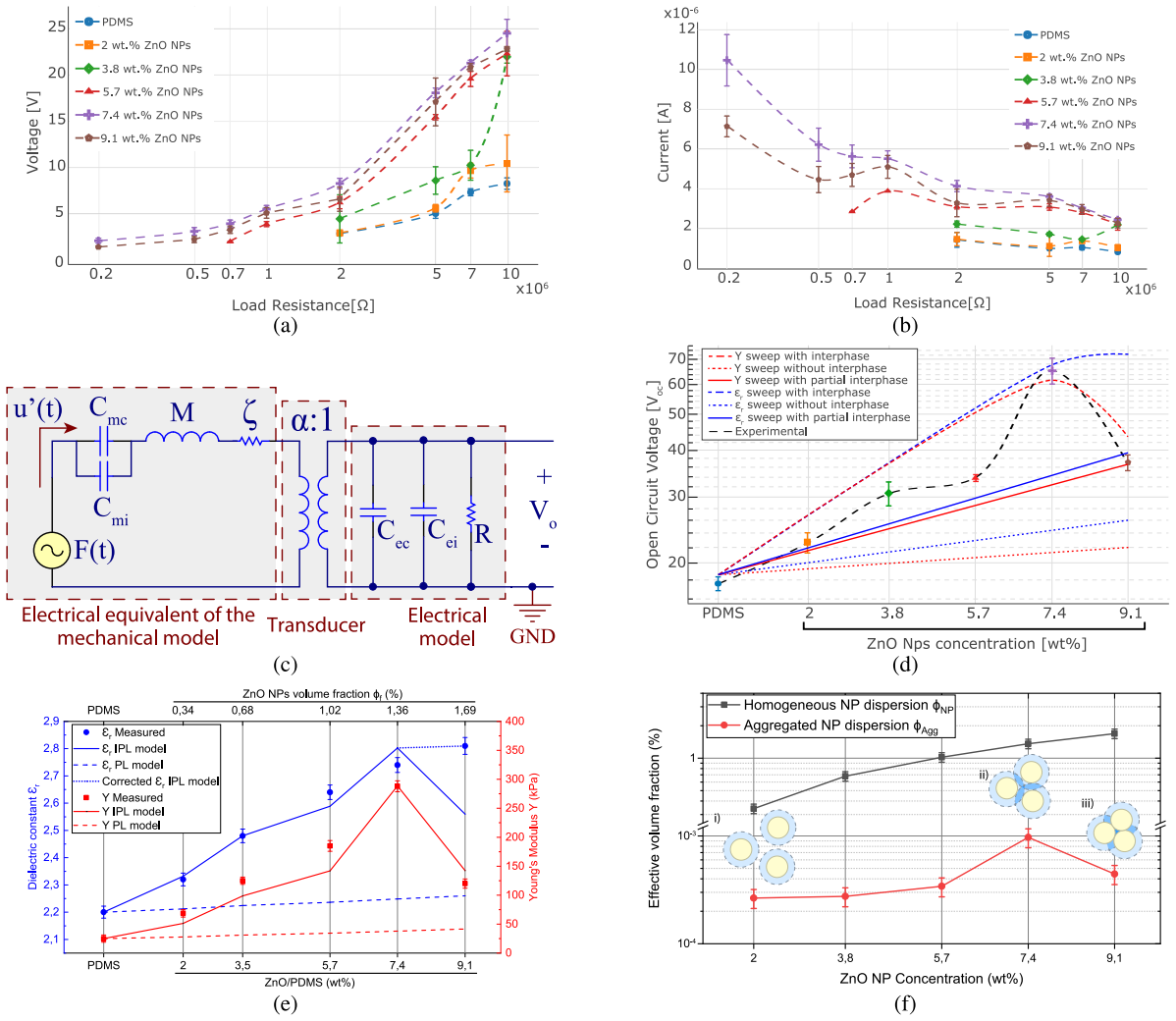

Fig. 3. Nanocomposite generator's energy conversion characterization and modeling are shown in: (a) Output voltage vs load resistance, (b) output current vs load resistance for five different ZnO NPs concentration and a pure PDMS film, (c) lumped element model composed of tree sections: the electrical equivalent of the mechanical model, the transducer with electromechanical coupling α, and the electrical model. (d) Nanocomposite generator's output voltage as a function of ZnO NPs concentration by variation of the dielectric constant ε (blue line), Young's modulus Y (red line) without considering the interphase contribution (ϕ_i=0) (dotted), with partial interphase contribution (ϕ_i at 50%) (solid), and complete interphase contribution (dashed). Experimental measurements (black long dashed line). (e) Young's modulus estimation (red squares) Dielectric constant estimation (blue circles) and its calculation by PL model (dotted line) and IPL model (solid line) as function of filler concentration, (f) Effective volume fraction vs ZnO NPs concentration for ZnO NPs considering an homogeneous dispersion (black squares) and aggregated ZnO NPs according to aggregation dispersion obtained from optical microscopy images (red circles), three levels of interactions between NPs (in yellow) and interphases (in blue) are shown in internal images: (i) no-interaction, (ii) interaction, (iii) overlapping.

The effect of the electromechanical properties of the nanocomposite on V_{oc} was studied using a LE model (Graton et al., 2013). Fig. 3(c) shows the model of the nanocomposite generator with three stages: (i) the mechanical equivalent for the nanocomposite is represented by the electrical equivalent of the damped oscillatory system (Caliò et al., 2014), (ii) electromechanical energy conversion by the transducer, and (iii) nanocomposite's electrical properties by the electrical model. The equivalent circuit of the mechanical model is fed by the applied force ($F(t)$), represented as a time-dependent voltage source, the derivative of the vertical strain ($u(t)$) as the current flowing in the circuit, C_{mc} and C_{mi} as a capacitance proportional to the constituents and interphase, M as the inductance linked to the nanocomposite's mass, and ζ as the mechanical damping ratio. The electromechanical transducer is a transformer, where α corresponds to the electromechanical coupling. The electrical model connected to the transformer is composed of C_{ec}, C_{ei} and R, representing the static capacitances that depend on ε_r of the nanocomposite's constituents and interphase, and the insulation resistance of the set of nanocomposite and electrodes. The model reveals information regarding the effect of the properties in the energy conversion process; the resistive elements ζ and R are the properties related to the mechanical and electrical losses, while the inductive and capacitive elements M, C_{mc}, C_{mi}, C_{ec}, and C_{ei} are the properties related to the mechanical and electrical energy storage. The circuit topology shows a second-order filter cascaded by a first-order filter configuration indicating an optimal Y and ε_r for the input $F(t)$ to obtain the maximum output V_{oc} set by properties of the nanocomposite.

Fig. 3(d) shows the open-circuit voltage V_{oc} as a function of the filler concentration in the nanocomposite for Y and ε_r sweeps using the LE model. Open circuit voltages produced were measured at 15 min of continuous excitation of the nanocomposite (see supplementary materials, Figure S2), here an increase of voltage was detected at 5 min for 2 wt% and 3.8 wt%, at 5 min, 10 min, 15 min for 5.7 wt%, 7.4 wt%, and 9.1 wt%. In contrast, the voltage of the PDMS sample without ZnO NPs did not increase with time. The voltage increase with time can be related to the reorganization of the filler aggregates in the nanocomposite. These results show the need for an additional more detailed characterization at the interface that can correlate the aggregation of the ZnO

NPs and the increase in the output voltage (Voc). The PDMS film produced a V_{oc} of 12 V, as the ZnO concentration increased to 7.4 wt%, the voltage rose to 65 V and fell to 36 V for 9.1 wt% filler concentration. The peak to peak voltage of the 7.4 wt% sample was measured at over 150 V (see supplementary materials, Figure S4), which is similar to other values from the literature while having aggregate formation during the fabrication process (See supplementary materials, Figure S5).

The data measured for Y and ε_r was fed into the model to obtain the output voltage for variation of Y using the PDMS' $\varepsilon_r = 2.2$ as a constant, and variation of ε_r using the PDMS' Y as constant. The model simulation exhibits a voltage increase at ε_r and Y variation up to a 5.7 wt% filler concentration. At 7.4 wt% and 9.1 wt% the simulation diverges, Y variation voltage saturates to 72 V, while ε variation voltage peaks to 58 V and drops to 45 V.

The model for the Y variation and ε_r variation correspond to the effect of the α, C_{mc}, C_{mi}, C_{ec}, and C_{ci} parameters. At increasing concentrations up to 7.4 wt%, three contributions to the voltage are considered. Firstly, the addition of ZnO NPs increases the number of elements that can provide electromechanical energy conversion via the piezoelectric effect and causes the electromechanical coupling α to increase. Secondly, an increase of Y in the interphase allows for less deformation to be absorbed by the matrix and more to be transferred to the ZnO NPs, increasing charge generated by the piezoelectric effect. Thirdly, the ε_r rise allows for a superior polarization in the nanocomposite. The increased α and Y generate enough charge formation to increase the output voltage at the corresponding ε_r value.

In contrast, at concentrations from 7.4 wt% to 9.1 wt%, while ε_r continues increasing, which increments the nanocomposite's charge required to produce higher voltages (Nelson, 2010), and Y decreases causing the softening of the nanocomposite allowing for more deformation of the PDMS matrix and a reduced deformation transferred to the ZnO NPs. The lower Y causes a reduction of the generated charge, which is not enough to maintain the higher voltages at the increased ε_r causing a voltage drop at higher concentrations.

Fig. 3(e) exhibits the estimated values for the nanocomposite's Y and ε_r at different filler concentrations. At concentrations between 2 wt% to 7.4 wt%, Y value increased from 25 kPa to 278 kPa, while at the 9.1 wt% concentration, Y decreased by 59%. On the other hand, ε_r increased from 2.20 in the pure PDMS films to 2.87 in the nanocomposite with 9.1 wt% filler concentration. The measurement of these electromechanical properties shows a non-constant increase of ε_r with the concentration. This can be affected by the contribution of the interphase that depends on the random dispersion and aggregation effect in addition to the contributions of the PDMS matrix and ZnO NPs filler. The interphase is defined as the region affected by filler–matrix and filler–filler interactions that produce a sharp finite region around the NPs with different properties matrix and filler (Deng and Van Vliet, 2011). The effect of the interphase was studied by the application of a PL and IPL models. The PL model considers the nanocomposite as a two-phase material where properties depend on the filler and matrix properties contribution, volume fraction (ϕ_i), and filler shape. On the other hand, the IPL model considers the ZnO/PDMS interphase as the third phase with different properties contributing to the properties of the nanocomposites (Todd and Shi, 2005). Similar studies have demonstrated the dependence of the interphase region on the filler's size, concentration, and dispersion (Ozmusul and Picu, 2002; Qu and Wong, 2002; Vo and Shi, 2002; Vo et al., 2001; Todd and Shi, 2002; Ma et al., 2017).

Fig. 3(f) shows the estimated effective volume fraction of the aggregated filler in the nanocomposite ϕ_{Agg} compared to the theoretical volume fraction of a homogeneously distributed filler ϕ_{NP}. The effective volume fraction describes the interphase volume of the nanocomposite, which is calculated from Eq. (2).

$$\phi_{Agg} = \left(\frac{D_{NP}}{D_{Agg}}\right)^{\frac{1}{3}} \phi_{NP} \tag{2}$$

Here, ϕ_{Agg} relates the volume fraction of the NPs, and D_{NP} and D_{Agg} to the mean diameters of NPs and aggregates, respectively. D_{Agg} was estimated by analysis of optical microscopy images, which exhibited the random dispersion and aggregation of the filler in the PDMS matrix (see supplemental materials, Figure S6). ϕ_{NP} shows a monotonic increase with the concentration while ϕ_{Agg} increases up to 7.4 wt% and then decreases at 9.1 wt%. This variation of ϕ_{Agg} is related to the region type of interaction between interphases and NPs. The levels of interaction present at each concentration are shown in the internal images. At concentrations of 2 wt% the low volume occupied by the filler and low aggregation allows for the prevalence of individual interphase regions with a high distance between particles that allow minimal interaction between interphases (Fig. 3(f)-i). Therefore, the interphase's contribution to the properties is set by the properties of the interphase and limited by low filler concentration. At increasing concentrations up to 7.4 wt%, the interphases shift to a level where the increased volume occupied by NPs and the higher aggregation reduce the distance between NPs into what is known as interphase interaction region and cause an intersection of the interphases that can exhibit even higher properties than the individual interphases (Fig. 3(f)-ii). At the maximum measured concentration of 9.1 wt%, the high concentration and short distance between NPs cause the formation of agglomerates which result in overlapping regions where NPs occupy the interphase volume decreasing ϕ_{agg}, hence affecting their contribution to the nanocomposite (Fig. 3(f)-iii). Generally, at homogenous dispersions, the effect of the interaction and overlapping phases is only expected at high filler concentrations that occupy over half of the nanocomposite volume. However, the presence of strong aggregation in our samples shifted the concentration that produces these levels to the low concentrations produced.

Additional analyses of the aggregates at 7.4 wt% were carried by multiple techniques. A Raman spectroscopy analysis (see supplementary materials, Figure S7) revealed the presence of aggregates at low depth in the nanocomposite. In contrast, XPS spectra analysis of the nanocomposite carried after the piezoelectric characterization revealed that the ZnO filler was only detectable after 5 μm etching, showing the absence of ZnO NPs in the top and bottom surfaces of the nanocomposite (see supplementary materials, Figure S8). These results indicate that at the range of 2 wt% to 7.4 wt%, the inclusion of ZnO NPs in the increasing concentrations dominates over aggregation and hence boosts the interphase fraction as each added NP provides its interphase contribution and closeness between NPs is not enough to produce interphase neglection caused by overlapping. This is confirmed by the TEM characterization that reveals aggregates that present both NP aggregates and interphase interaction (see supplementary materials, Figures S9, S10). Conversely, at the concentration of 9.1 wt%, the aggregation increased by the combined effect of reduced interparticle distance and polar incompatibility between polar ZnO and non-polar PDMS created large ZnO NPs aggregates dominated by NP aggregates which resulted in the reduced interphase by the effect of its overlapping, hence, dominating over the concentration.

The estimated ϕ_{Agg} value is used to calculate the effect of the interphase in the PL and IPL models described in Eq. (3) and (4), respectively.

$$P_c^{\beta} = \phi_m P_m^{\beta} + \phi_f P_f^{\beta} \tag{3}$$

$$P_c^{\beta} = \phi_m P_m^{\beta} + \phi_i P_i^{\beta} + \phi_f P_f^{\beta} \tag{4}$$

Wherein P is defined as the studied property (ε_r or Y), ϕ is the volume fraction, β a dimensionless parameter describing the shape and orientation of the filler particles, and the subindex identifies composite (c), matrix (m), filler (f), or filler–matrix interphase (i). The PDMS matrix ε_r corresponds to the experimental measurements of 2.2. The Young's modulus of PDMS of 25 kPa, ZnO ε_r of 8.75 and Y of 111.2 GPa values were obtained from the literature (Rossler, 2013a,b). The ϕ_f was calculated from the ZnO filler concentration, ϕ_i from ϕ_{Agg}, and ϕ_m from the remaining volume. The interphase properties P_i and the β parameter were optimized to fit the experimental data, resulting in a Y_i value of 550 kPa, and a ε_i of 6.59 both values higher than pristine PDMS. The optimized value β value of 0.24 corresponds to a horizontally elongated ellipsoid NPs mean shape (Todd and Shi, 2005). The effect of the interphase shown in the models correspond with previous studies where the effect of ZnO nanostructures was identified in mechanical (Jin et al., 2014), and piezoelectric properties (Zhang et al., 2020).

The ε_r and Y measurements show that the IPL models error is inferior to the PL model, thus indicating that the nanocomposite properties depend on the interphase properties in addition to the ZnO and PDMS properties. The interphase Y value can be a result of interactions during and after cross-linking (Putz et al., 2008). During this process, the chemical interactions between ZnO and PDMS cause a significant increase in the formation of siloxane covalent (Si-O-Si) bonds during the hydrosilylation reaction between the PDMS base and curing agent (Bistričić et al., 2013), this result in attraction forces up to ten times stronger than the weaker hydrogen bonds they replace, increasing Y value (Jeffrey and Saenger, 1991). After curing, the interactions can be classified into two types: Firstly, the filler–matrix interaction, where Van der Waals dispersion forces between the polar ZnO NPs and non-polar PDMS affect the polymer chains by constraining its stretching, twisting, and wagging, increasing the stiffness of the matrix around the NPs and rising Y (Todd and Shi, 2005; Israelachvili, 2011). Secondly, the added polar interactions between NPs can cause aggregation zones and segregated polymer volumes that can affect the nanocomposites mechanical properties (Deng and Van Vliet, 2011; Israelachvili, 2011).

Regarding ε_r, the IPL model captures the experimental data with an optimized interphase value of 6.59 higher than PDMS (2.20) and an interphasial volume that increases 2.8 times from 2 wt% to 7.4 wt% and decreases by 45% from 7.4 wt% to 9.1 wt%. The error between the IPL model and the measurements is under 1% up to a 3.8 wt% filler concentration and increases to 8.9% at 9.1 wt% concentration. Compared to the PL model, the closeness between the IPL model and the measurements shows that the effect of the interphase is required to explain the nanocomposites ε_r value. The interphase contribution can be caused by a polarization formed by the difference in ZnO and PDMS properties as ε_r value that limits the charge transfer in the interphase, causing its build-up (also known as Maxwell–Wagner–Sillars or MWS polarization) (Dang, 2013; Tsangaris et al., 1998; Kremer and Schönhals, 2003) which causes an ε_r increment. The increased error at the 9.1 wt% concentration indicates increased agglomerations and reduced effective volume fraction. However, other mechanisms can produce interphases that are not considered within the model and need to be explored in future work. To fit this ε_r value, an increase of the interphase in 1.7 times is required and can be explained by the interaction of neighboring NPs ε_r that create regions with an increased electric flux that enhance the ε_r value in the NP to NP interphase (Jin and Gerhardt, 2016). This effect caused by filler–filler interactions is dominant at higher concentrations and uneven distribution, reducing the distance between NPs increasing the interphase region and is not considered by the IPL model, which only includes the effect of filler–matrix interactions.

The integration to the lumped model of the electromechanical properties obtained from the PL model without considering the interphase contribution reveals increased in with the output voltage compared to the experimental values that correspond to the IPL model that includes the interphase contribution. If partial or complete interphase is considered, the difference between the generated voltages is reduced, indicating that the increased young modulus from the interphase interactions between filler and matrix produce a more significant enhancement of the voltage generation of the nanocomposite. The detected high voltage, Y, and effective volume fraction exhibited in the 7.4 wt% concentration sample with random dispersion indicate that at these concentrations the formation of the interphase reaches it maximum value caused by the added NPs and that at increasing concentrations the aggregation causes an interphase reduction that reduces these values. IPL modeling of the nanocomposite indicates that to capture the modulus' experimental measurements, the interphase region should exhibit an average Y value 22 times superior to the PDMS value at a degree of aggregation that allows for the formation of aggregates to be not compact enough to produce a significative reduction on the interphase by the effect of overlapping. This superior Y value that results in a hardening effect on the interphase proves to be beneficial to the energy conversion process as it allows for inferior energy absorption on the PDMS matrix and superior strain transference to the ZnO NPs, enhancing the polarization by the piezoelectric effect.

We are currently developing a simplified ZnO-PDMS molecular surface structure model to explore the dynamic evolution of local polarization as a function of strain (compressive and shear) using ab initio molecular dynamics with the VASP code (Vienna Ab initio Simulation Package) (Kresse and Hafner, 1993). We expect this will contribute further understanding about the key mechanisms at play in our experimental setup, and provide structural cues into the optimization of structure and composition for improved piezoelectric response in ZnO-PDMS composites.

4. Conclusions

The effect of the interphase in the output voltage of a Zn0/PDMS nanocomposite generator at low concentrations ($<$10 wt%) and random dispersion was studied. The nanocomposite generator produced maximum a peak-to-peak voltage of $\approx$150 V that is comparable to previous literature values in homogeneous nanocomposites. This voltage is produced due to the effect interacting interphases present in the aggregates produced by random dispersion. Also, three levels of interface interactions were identified in the experimental data visible at concentrations between 2 wt% to 9.1 wt%. The individual interphases level present at concentrations of 2 wt% which produced a peak voltage of $\approx$23 V. The interacting interphases level was exhibited at 7.4 wt% and exhibited the highest voltage with an increase of 6 times. The overlapping between NPs and interfaces was most notable at 9.4 wt% where its diminishing effect on the effective volume fraction caused a reduction of 40% of the output voltage. Additionally, the IPL and LE models describe the electromechanical properties and also captured the tendency of the generated voltages. The presented results demonstrate the critical importance of the interacting interphase in the design of ZnO/PDMS nanocomposite generators for high voltage generation at low concentration and random dispersion conditions.

Declaration of competing interest

The authors declare that they have no known competing financial interests or personal relationships that could have appeared to influence the work reported in this paper.

Acknowledgments

J.A. Perez-Taborda and J.M. Marmolejo-Tejada acknowledge the financial support from *Department of Science, Technology, and Innovation (Colciencias)* fellowship for the grant agreement N°.808. The authors wish also to thank the researchers Dr. Elvis Lopez and Dr. A. Mello for XPS measurements at the Laboratory of Surface and Nanostructures, Brazilian Physical Research Center - RJ, Brazil.

Funding

This work was supported by Minciencias (Colombia) under Grant 808-2018 and a Joint Research Grant Program (2018) *"Convocatoria interinstitucional de investigación en Ingeniería"* between the Pontificia Universidad Javeriana Cali and Universidad de los Andes.

Appendix A. Supplementary data

Supplementary material related to this article can be found online at https://doi.org/10.1016/j.egyr.2021.01.086.

References

Abbas, M., Buntinx, M., Deferme, W., Peeters, R., 2019. (Bio)polymer/ZnO nanocomposites for packaging applications: A review of gas barrier and mechanical properties. Nanomaterials 9 (10), 1–14. http://dx.doi.org/10.3390/nano9101494.

Avila, A., Perez-Taborda, J.A., Perez-Lopez, C.A., 2020. AITAAVAPP.

Bistričić, L., Borjanović, V., Mikac, L., Dananić, V., 2013. Vibrational spectroscopic study of poly(dimethylsiloxane)-ZnO nanocomposites. Vib. Spectrosc. 68, 1–10. http://dx.doi.org/10.1016/j.vibspec.2013.05.005.

Caliò, R., Rongala, U.B., Camboni, D., Milazzo, M., Stefanini, C., de Petris, G., Oddo, C.M., 2014. Piezoelectric energy harvesting solutions. Sensors 14 (3), 4755–4790. http://dx.doi.org/10.3390/s140304755, URL: http://www.mdpi.com/1424-8220/14/3/4755.

Chen, J., Wang, Z.L., 2017. Reviving vibration energy harvesting and self-powered sensing by a triboelectric nanogenerator. Joule 1 (3), 480–521. http://dx.doi.org/10.1016/j.joule.2017.09.004, URL: https://linkinghub.elsevier.com/retrieve/pii/S2542435117300776.

Dang, Z.M., 2013. Polymer nanocomposites with high permittivity. In: Nanocrystalline Materials: Their Synthesis-Structure-Property Relationships and Applications, second ed. Elsevier Ltd, pp. 305–333. http://dx.doi.org/10.1016/B978-0-12-407796-6.00009-9.

Deng, F., Van Vliet, K.J., 2011. Prediction of elastic properties for polymer–particle nanocomposites exhibiting an interphase. Nanotechnology 22 (16), 165703. http://dx.doi.org/10.1088/0957-4484/22/16/165703, URL: https://iopscience.iop.org/article/10.1088/0957-4484/22/16/165703.

Diaz, A., Felix-Navarro, R., 2004. A semi-quantitative tribo-electric series for polymeric materials: the influence of chemical structure and properties. J. Electrost. 62 (4), 277–290. http://dx.doi.org/10.1016/j.elstat.2004.05.005, URL: https://linkinghub.elsevier.com/retrieve/pii/S0304388604001287.

Ding, X., Cao, H., Zhang, X., Li, M., Liu, Y., 2018. Large scale triboelectric nanogenerator and self-powered flexible sensor for human sleep monitoring. Sensors 18 (6), 1713. http://dx.doi.org/10.3390/s18061713, URL: http://www.mdpi.com/1424-8220/18/6/1713.

Giannuzzi, L.A., Drown, J.L., Brown, S.R., Irwin, R.B., Stevie, F.A., 1998. Applications of the FIB lift-out technique for TEM specimen preparation. Microsc. Res. Tech. 41 (4), 285–290. http://dx.doi.org/10.1002/(SICI)1097-0029(19980515)41:4<285::AID-JEMT1>3.0.CO;2-Q.

Graton, O., Poulin-Vittrant, G., Dahiya, A.S., Camara, N., Hue, L.P.T.H., Lethiecq, M., 2013. Equivalent circuit model of a nanogenerator based on a piezoelectric nanowire-polymer composite. Phys. Status Solidi - Rapid Res. Lett. 7 (10), 915–918. http://dx.doi.org/10.1002/pssr.201308017.

Hasan, M.R., Baek, S.-H., Seong, K.S., Kim, J.H., Park, I.-K., 2015. Hierarchical ZnO nanorods on Si micropillar arrays for performance enhancement of piezoelectric nanogenerators. ACS Appl. Mater. Interfaces 7 (10), 5768–5774. http://dx.doi.org/10.1021/am5085379, URL: http://pubs.acs.org/doi/10.1021/am5085379.

Israelachvili, J.N., 2011. Interactions involving polar molecules. In: Intermolecular and Surface Forces. Elsevier, pp. 71–90. http://dx.doi.org/10.1016/B978-0-12-375182-9.10004-1, URL: https://linkinghub.elsevier.com/retrieve/pii/B9780123751829100041.

Jang, J.-S., Bouveret, B.t., Suhr, J., Gibson, R.F., 2012. Combined numerical/experimental investigation of particle diameter and interphase effects on coefficient of thermal expansion and young's modulus of SiO2/epoxy nanocomposites. Polym. Compos. 33 (8), 1415–1423. http://dx.doi.org/10.1002/pc.22268, URL: http://doi.wiley.com/10.1002/pc.22268.

Jeffrey, G.A., Saenger, W., 1991. Hydrogen Bonding in Biological Structures. Springer Berlin Heidelberg, Berlin, Heidelberg, http://dx.doi.org/10.1007/978-3-642-85135-3, URL: http://link.springer.com/10.1007/978-3-642-85135-3.

Jin, X., Deng, M., Kaps, S., Zhu, X., Hölken, I., Mess, K., Adelung, R., Mishra, Y.K., 2014. Study of tetrapodal ZnO-PDMS composites: A comparison of fillers shapes in stiffness and hydrophobicity improvements. In: Gan, Y. (Ed.), PLoS One 9 (9), e106991. http://dx.doi.org/10.1371/journal.pone.0106991, URL: https://dx.plos.org/10.1371/journal.pone.0106991.

Jin, Y., Gerhardt, R.A., 2016. Simulation of the effects of nano-filler interactions in polymer matrix dielectric nanocomposites. In: 2016 COMSOL Conference, p. 7.

Kremer, F., Schönhals, A. (Eds.), 2003. Broadband Dielectric Spectroscopy. Springer Berlin Heidelberg, Berlin, Heidelberg, http://dx.doi.org/10.1007/978-3-642-56120-7, URL: http://link.springer.com/10.1007/978-3-642-56120-7.

Kresse, G., Hafner, J., 1993. Ab initio molecular dynamics for liquid metals. Phys. Rev. B 47 (1), 558–561. http://dx.doi.org/10.1103/PhysRevB.47.558, URL: https://link.aps.org/doi/10.1103/PhysRevB.47.558.

Kumar, B., Kim, S.W., 2012. Energy harvesting based on semiconducting piezoelectric ZnO nanostructures. Nano Energy 1 (3), 342–355. http://dx.doi.org/10.1016/j.nanoen.2012.02.001.

Latif, I., E. AL-Abodi, E., H. Badri, D., Al Khafagi, J., 2013. Preparation, characterization and electrical study of (carboxymethylated polyvinyl alcohol/ZnO) nanocomposites. Am. J. Polym. Sci. 2 (6), 135–140. http://dx.doi.org/10.5923/j.ajps.20120206.01.

Liu, Z., Moore, J.A., Liu, W.K., 2016. An extended micromechanics method for probing interphase properties in polymer nanocomposites. J. Mech. Phys. Solids 95, 663–680. http://dx.doi.org/10.1016/j.jmps.2016.05.002.

Ma, X., Zare, Y., Rhee, K.Y., 2017. A two-step methodology to study the influence of aggregation/agglomeration of nanoparticles on Young's modulus of polymer nanocomposites. Nanoscale Res. Lett. 12, 0–6. http://dx.doi.org/10.1186/s11671-017-2386-0.

Nelson, J.K. (Ed.), 2010. Dielectric Polymer Nanocomposites. Springer US, Boston, MA, http://dx.doi.org/10.1007/978-1-4419-1591-7, URL: http://link.springer.com/10.1007/978-1-4419-1591-7.

Netravali, A., Mittal, K.L. (Eds.), 2017. Interface / Interphase in Polymer Nanocomposites. Willey.

Ozmusul, M.S., Picu, R.C., 2002. Elastic moduli of particulate composites with graded filler-matrix interfaces. Polym. Compos. 23 (1), 110–119. http://dx.doi.org/10.1002/pc.10417.

Parangusan, H., Ponnamma, D., Al Ali Almaadeed, M., 2017. Flexible tri-layer piezoelectric nanogenerator based on PVDF-HFP/Ni-doped zno nanocomposites. RSC Adv. 7 (79), 50156–50165. http://dx.doi.org/10.1039/c7ra10223b.

Parangusan, H., Ponnamma, D., Al-Maadeed, M.A.A., 2018. Stretchable electrospun PVDF-HFP/Co-ZnO nanofibers as piezoelectric nanogenerators. Sci. Rep. 8 (1), 1–11. http://dx.doi.org/10.1038/s41598-017-19082-3.

Pradel, K.C., Wu, W., Ding, Y., Wang, Z.L., 2014. Solution-Derived ZnO homojunction nanowire films on wearable substrates for energy conversion and self-powered gesture recognition. Nano Lett. 14 (12), 6897–6905. http://dx.doi.org/10.1021/nl5029182.

Putz, K.W., Palmeri, M.J., Cohn, R.B., Andrews, R., Brinson, L.C., 2008. Effect of cross-link density on interphase creation in polymer nanocomposites. Macromolecules 41 (18), 6752–6756. http://dx.doi.org/10.1021/ma800830p, URL: https://pubs.acs.org/doi/10.1021/ma800830p.

Qu, J., Wong, C.P., 2002. Effective elastic modulus of underfill material for flip-chip applications. IEEE Trans. Compon. Packag. Technol. 25 (1), 53–55. http://dx.doi.org/10.1109/6144.991175.

Raja, S.N., Olson, A.C.K., Limaye, A., Thorkelsson, K., Luong, A., Lin, L., Ritchie, R.O., Xu, T., Alivisatos, A.P., 2015. Influence of three-dimensional nanoparticle branching on the Young's modulus of nanocomposites: Effect of interface orientation. Proc. Natl. Acad. Sci. 112 (21), 6533–6538. http://dx.doi.org/10.1073/pnas.1421644112, URL: http://www.pnas.org/lookup/doi/10.1073/pnas.1421644112.

Rossler, U., 2013a. ZnO: dielectric constant, effective charge. In: New Data and Updates for Several Semiconductors with Chalcopyrite Structure, for Several II-VI Compounds and Diluted Magnetic IV-VI Compounds. Springer Berlin Heidelberg, Berlin, Heidelberg, pp. 171–175. http://dx.doi.org/10.1007/978-3-642-28531-8_84.

Rossler, U., 2013b. ZnO: Young's modulus. In: New Data and Updates for Several Semiconductors with Chalcopyrite Structure, for Several II-VI Compounds and Diluted Magnetic IV-VI Compounds. Springer Berlin Heidelberg, Berlin, Heidelberg, p. 170. http://dx.doi.org/10.1007/978-3-642-28531-8_83.

Schindelin, J., Arganda-Carreras, I., Frise, E., Kaynig, V., Longair, M., Pietzsch, T., Preibisch, S., Rueden, C., Saalfeld, S., Schmid, B., Tinevez, J.-Y., White, D.J., Hartenstein, V., Eliceiri, K., Tomancak, P., Cardona, A., 2012. Fiji: an open-source platform for biological-image analysis. Nature Methods 9 (7), 676–682. http://dx.doi.org/10.1038/nmeth.2019, URL: http://www.nature.com/articles/nmeth.2019.

Song, P., Yang, G., Lang, T., Yong, K.-T., 2019. Nanogenerators for wearable bioelectronics and biodevices. J. Phys. D: Appl. Phys. 52 (2), 023002. http://dx.doi.org/10.1088/1361-6463/aae44d, URL: http://stacks.iop.org/0022-3727/52/i=2/a=023002?key=crossref.67e44534f826b06e42c6a54788a2ffae.

Technologies, K., 2014. Keysight 16451B Dielectric Test Fixture, sixth ed. Keysight Technologies.

Todd, M.G., Shi, F.G., 2002. Validation of a novel dielectric constant simulation model and the determination of its physical parameters. Microelectron. J. 33 (8), 627–632. http://dx.doi.org/10.1016/S0026-2692(02)00038-1, URL: https://linkinghub.elsevier.com/retrieve/pii/S0026269202000381.

Todd, M.G., Shi, F.G., 2005. Complex permittivity of composite systems: A comprehensive interphase approach. IEEE Trans. Dielectr. Electr. Insul. 12 (3), 601–611. http://dx.doi.org/10.1109/TDEI.2005.1453466.

Tsangaris, G.M., Psarras, G.C., Kouloumbi, N., 1998. Electric modulus and interfacial polarization in composite polymeric systems. J. Mater. Sci. 33 (8), 2027–2037. http://dx.doi.org/10.1023/A:1004398514901.

Vo, H.T., Shi, F.G., 2002. Towards model-based engineering of optoelectronic packaging materials: dielectric constant modeling. Microelectron. J. 33 (5–6), 409–415. http://dx.doi.org/10.1016/S0026-2692(02)00010-1, URL: https://linkinghub.elsevier.com/retrieve/pii/S0026269202000101.

Vo, H.T., Todd, M., Shi, F.G., Shapiro, A.A., Edwards, M., 2001. Towards model-based engineering of underfill materials: CTE modeling. Microelectron. J. 32 (4), 331–338. http://dx.doi.org/10.1016/S0026-2692(00)00152-X.

Xu, S., Qin, Y., Xu, C., Wei, Y., Yang, R., Wang, Z.L., 2010. Self-powered nanowire devices. Nature Nanotechnol. 5 (5), 366–373. http://dx.doi.org/10.1038/nnano.2010.46.

Zare, Y., 2016. Study of nanoparticles aggregation/agglomeration in polymer particulate nanocomposites by mechanical properties. Composites A 84, 158–164. http://dx.doi.org/10.1016/j.compositesa.2016.01.020.

Zhang, X., Le, M.-Q., Zahhaf, O., Capsal, J.-F., Cottinet, P.-J., Petit, L., 2020. Enhancing dielectric and piezoelectric properties of micro-ZnO/PDMS composite-based dielectrophoresis. Mater. Des. 192, 108783. http://dx.doi.org/10.1016/j.matdes.2020.108783, URL: https://linkinghub.elsevier.com/retrieve/pii/S0264127520303178.

Zhang, X., Li, B.W., Dong, L., Liu, H., Chen, W., Shen, Y., Nan, C.W., 2018. Superior energy storage performances of polymer nanocomposites via modification of filler/polymer interfaces. Adv. Mater. Interfaces 5 (11), 1–28. http://dx.doi.org/10.1002/admi.201800096.